The fracture mechanism of circular/elliptical concrete rings under restrained shrinkage and drying from top and bottom surfaces

Wei Dong[1, *], Wenyan Yuan[2], Xiangming Zhou[3], Fulu Wang[4]

1. Associate Professor, State Key Laboratory of Coastal and Offshore Engineering, Dalian University of Technology, Dalian 116024, P. R. China.

(*Corresponding author) E-mail: dongwei@dlut.edu.cn

2. Postgraduate student, State Key Laboratory of Coastal and Offshore Engineering, Dalian University of Technology, Dalian 116024, P. R. China.

E-mail: yuanwenyan@mail.dlut.edu.cn

3. Reader in Civil Engineering Design, Department of Mechanical, Aerospace and Civil Engineering, Brunel University London, Uxbridge UB8 3PH, UK.

E-mail:xiangming.zhou@brunel.ac.uk

4. Postgraduate student, State Key Laboratory of Coastal and Offshore Engineering, Dalian University of Technology, Dalian 116024, P. R. China.

E-mail: wangfulu@mail.dlut.edu.cn

Abstract:

Due to uniform shrinkage along the radial direction, drying from both top and bottom surfaces has been recommended to replace drying from outer circumference surface in the restrained circular ring test to assess cracking tendency of concrete. However, non-uniform shrinkage along the height direction under drying conditions is significant, and its effect on crack initiation and propagation in a concrete ring is not clearly understood. To investigate the fracture mechanism of the restrained ring test under drying from top and bottom surfaces, three series of circular and elliptical ring specimens with heights of 30 mm, 50 mm and 75 mm are tested to measure the cracking ages. A fracture mechanics based numerical method is proposed by introducing fictitious crack model to simulate the fracture process and predict the cracking age of a concrete ring under restraint. The effects of ring geometric profile, specimen height and moisture gradient on crack development are discussed. The results indicate that, under drying from both top and bottom surfaces, crack initiates partly along the height direction at the inner circumference of a concrete ring, and propagates along the radial direction, one by one, until the crack propagated throughout the whole cross-section. The moisture gradient along the height direction has significant effect on the crack driving force, which is dominated by the moisture gradient and steel ring restraint near the exposed surface, whose proportion increases with the increase in distance from the exposed surface.

Keywords: ring test; restrained shrinkage; concrete cracking; crack propagation; drying condition.

Nomenclature

A_1, A_2, B_1, B_2	coefficients for moisture distribution
D	distance from drying surface
E	elastic modulus
f_t	splitting tensile strength
G_f	fracture energy
$H_{EXPOSED}$	relative humidity at the exposed surface of the specimen
$H_{INTERNAL}$	internal relative humidity of the concrete specimen if it is completely sealed
K_{IC}^{ini}	initial fracture toughness
K_I^S	stress intensity factor caused by the shrinkage effect
$K_{I\ steel}^{S}$	stress intensity factor caused by steel restraint
K_I^{σ}	stress intensity factor caused by the cohesive stress
R_0	inner radius of a circular concrete ring
R_1	major inner radius of the elliptical concrete ring
R_2	minor inner radius of the elliptical concrete ring
t	age of concrete
w	crack opening displacement
w_0	stress-free crack opening displacement
w_s	displacement corresponding to the break point in the bilinear σ-w relationship
Δ	length of horizontal initial crack
σ	softening stress
σ_s	stress corresponding to the break point in the bilinear σ-w relationship

1 Introduction

Concrete is likely to experience shrinkage in response to cement hydration, temperature reduction and moisture dissipation in the process of maintenance, most notably at early ages. When the shrinkage is restrained, cracks initiate easily in concrete structures due to its low cracking resistance, resulting in low structure durability and significant maintenance costs [1]. Therefore, it is important to choose the appropriate laboratory test methods to assess the cracking tendency of concrete used in the field. So far, several test methods have been developed to assess cracking resistance of cementitious materials in the restrained condition, including restrained uniaxial test [2, 3], restrained slab test [4, 5], restrained beam test [6, 7], and restrained ring test [8-12]. Due to its relatively low cost and capacity of providing uniformity end restraint, the restrained ring test has been widely adopted over the other test methods for assessing cracking potential of concrete mixtures.

To standardize the restrained ring test, American Association of State Highway and Transportation Officials (AASHTO) (i.e. AASHTO PP34-99: Standard Practice for Cracking Tendency Using a Ring Specimen) recommended a certain version of ring specimen: a 75 mm thick concrete ring restrained by a 12.5 mm thick steel ring and dried from its outer circumferential surface. It was reported that, in some cases, the circular ring specimen recommended by AASHTO did not provide enough degree of restraint to enable the concrete to crack early enough [13]. In addition, the cracks would occur at the outer circumference and propagate into inner circumference as a result of non-uniform shrinkage along the radial direction caused by the moisture gradient [14, 15]. It has been certified that for a 75 mm thick concrete ring specimen drying from the outer circumferential surface, shrinkage cracking is mainly due to self-restraint caused by non-uniform shrinkage of the concrete ring itself rather than by external restraint from the central restraining steel ring [16]. In this case, the ring test results could not be used to determine the cracking tendency of concrete under restrained condition. Therefore, the American Society for Testing Material (ASTM) (i.e. ASTM C1581/C1581M-09a: Standard Test Method for Determining Age at Cracking and Induced Tensile Stress Characteristics of Mortar and Concrete under Restrained Shrinkage) suggested an improved ring specimen in which the thickness of concrete was reduced from 75 mm to 37.5 mm. Such improvement increases the relative restraint capacity of a steel ring, i.e. the external restrain, accelerates the occurrence of the first crack [17] and partly reduces non-uniform shrinkage along the radial direction. Radlinska et al. [18, 19] carried out numerous restrained ring tests following the ASTM standard to assess its accuracy and repeatability. The relatively small standard deviations in strain measurements indicated that the test method recommended by ASTM is reliable for ascertaining cracking susceptibility of cementitious systems. It is widely accepted that the minimum specimen size should be three times larger than the maximum aggregate size to ensure homogeneous concrete mixture. In the case of concrete mixture with larger aggregate sizes (such as 15 mm or 20 mm), the 37.5 mm thick concrete ring cannot meet this requirement [17].

Since it is hard to assess the cracking tendency of concrete ring specimens containing larger aggregates and drying from outer circumference under restrained shrinkage, the ring specimen drying from top and bottom surfaces was adopted [15, 17, 20-22]. The most significant advantage to allow drying from the top and bottom surfaces is that moisture diffuses simultaneously from two symmetrically exposed surfaces so that the moisture diffusion distance is the half of specimen height. It allows a concrete ring to be sufficiently thick to enable larger aggregates to be used. However, it should be noted that drying from top and bottom surfaces results in uniform shrinkage along the radial direction, but non-uniform shrinkage along the height direction. For a concrete ring with a small height (e.g. 30 mm), the moisture gradient and non-uniform shrinkage along its height direction can be neglected, and the uniform shrinkage assumption can be employed approximately [21, 22]. However, with the increase of specimen height, the moisture gradient along the height direction becomes more significant, which makes the shrinkage at the exposed surfaces obviously greater than that at the inner surface. Particularly, the non-uniform shrinkage along the height affects the crack initiation position and propagation direction in concrete. Further, it is difficult to define the crack status when the sudden decrease in the strain of the steel ring occurs in the ring test subject to drying from top and bottom surfaces. Aiming to determine the influence of the moisture gradient on the degree of restraint, Moon et al. [17] used numerical method to analyze the stress and strain distributions along the height direction of a 75 mm tall ring specimen under drying from top and bottom surfaces. However, to the best of the authors' knowledge, the crack initiation and propagation process in a concrete ring under drying from the top and bottom surfaces has not been reported. From the practical point of view, it is significant to have a better understanding of the failure mechanism of concrete, so that the ring test subject to top and bottom surfaces drying can be more effectively used in the assessment of cracking tendency of concrete with larger aggregates.

In addition, two analytical methods used in previous study to investigate the failure mechanism of a concrete ring in restrained ring test are the stress-based method [13, 20, 23] and the R-curve-based method [21-25], respectively. The advantage of the stress-based method is that the classical elastic theory can be employed to calculate the residual stress in concrete. It is convenient to develop the analytical formulas to calculate the stress distribution in a concrete ring. The R-curve method based on nonlinear elastic fracture mechanics was also used to interpret cracking of concrete in the ring test, which has been certified in the determination of critical crack propagation status. However, considering concrete as quasi-brittle material, there are three distinguished stages in the crack propagation process, i.e. crack initiation, stable propagation and unstable propagation [26]. Particularly, the crack propagation in a concrete ring becomes more complicated when the non-uniform shrinkage along the ring height is considered. In order to simulate the whole crack propagation process, the nonlinear fracture theory combined with fictitious crack mode would be more appropriate, because the nonlinear cohesive characteristic of concrete can be taken into account in this method [27].

Recently, the novel elliptical ring geometry [25, 28-30] was proposed as a supplement to the traditional circular ring geometry in the ring test, which can increase the restrained degree to concrete and accelerate the first crack occurrence. In addition, due to the influence of the elliptical geometry, the first crack usually occurs near major axis in an elliptical ring specimen, which is conveniently observed in the elliptical ring test. In order to investigate the fracture mechanics in the circular and elliptical rings under drying from the top and bottom surfaces, a nonlinear fracture mechanics-based method is developed in this research to simulate the restrained shrinkage effect on concrete and investigate the crack propagation process. The effect of non-uniform shrinkage along the height direction on fracture process is discussed through investigating circular and elliptical concrete rings with three heights, i.e. 30 mm, 50 mm and 75 mm. It is expected that the research conducted in this paper can reveal the failure mechanism in the ring test subject to drying from top and bottom surfaces, so that the circular and elliptical tests can be reasonably chosen in the assessment of cracking tendency for concrete with larger aggregates.

2 Experimental Programme

The basic mechanical properties, fracture properties and free shrinkage were investigated by conducting circular/elliptical ring tests in this study. The mix proportions for the concrete used in experiment were 1:1.5:1.5:0.5 (cement: sand: aggregate: water) by weight. The maximum size of the aggregate was 10 mm. After curing in normal laboratory environment for 24 h, the specimens were demoulded and moved into an environment chamber with 23℃ and 50% relative humidity (RH) for curing until the designated age of testing or cracking in cases of the ring test.

2.1 Tests on mechanical **and fracture properties of concrete**

Mechanical and fracture properties, including elastic modulus E, splitting tensile strength f_t, fracture energy G_f, and initial fracture toughness K_{IC}^{ini}, of concrete used in this study were measured at 1, 3, 5, 7, 14, 21 and 28 days respectively. Experimental data at various ages were fitted to continuous functions by regression analyses, which estimated the age-dependent relationships from 1 to 28 days (see Eqs. (1) to (4)). Here, t is the age of concrete in days.

$$E(t) = 13.8973 + 0.4t - 0.0056t^2 \qquad (t \le 28 \text{ days}) \tag{1}$$

$$f_t(t) = 1.224 + 0.44 \times \ln(t - 0.0318) \qquad (t \le 28 \text{ day} \tag{2}$$

$$G_f(t) = 41.39 + 10.35 \times \ln(t - 0.326) \qquad (t \le 28 \text{ day} \tag{3}$$

$$K_{IC}^{ini}(t) = -0.301 + 0.26 \times \ln(t + 0.272) \qquad (t \le 28 \text{ day} \tag{4}$$

The correlation coefficients of the above regression analyses are 0.926, 0.956, 0.872 and 0.947, respectively, which indicates that relevant concrete material properties at early ages can be determined from above equations with high accuracy.

2.2 Restrained circular/elliptical ring tests

In order to investigate the influence of non-uniform shrinkage along the height direction on fracture process of concrete in the ring test, three series of restrained ring specimens with different heights (30 mm, 50 mm and 75 mm) were tested in this study. For each series of ring specimens, two geometric profiles, i.e. circular and elliptical rings, were investigated in parallel to monitor the cracking ages of concrete.

The diagrams of the three series of ring specimens with different heights are shown as Fig. 1.

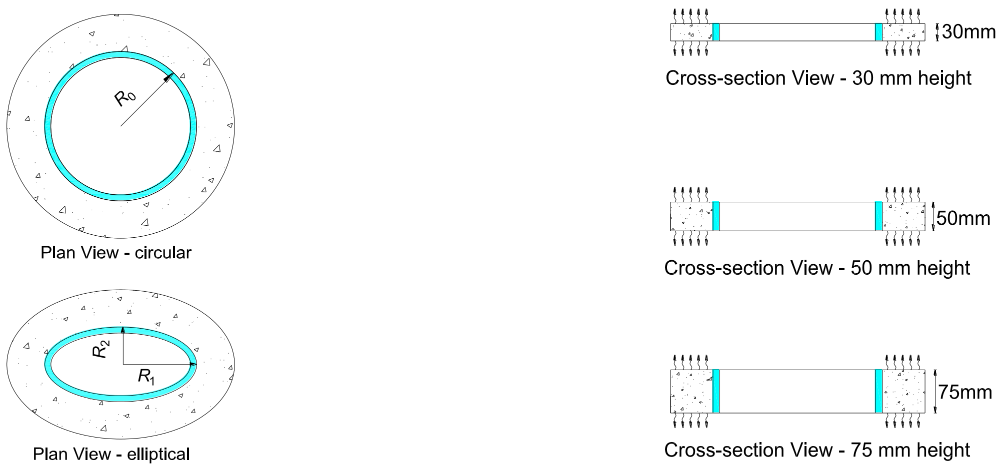

(a) Plan views of circular and elliptical ring specimens

(b) Cross-section views of ring specimens with 30 mm, 50 mm and 75 mm heights

Fig. 1. Diagrams of ring specimens.

The inner radius of a circular concrete ring is denoted as R_0, and the major and minor inner radii of an elliptical concrete ring are denoted as R_1 and R_2, respectively. According to previous research [29], the elliptical ring geometry with R_1/R_2 between 2 and 3 is the most effective in providing a high degree of restraint to initiate early concrete cracking. Therefore, for the ring specimens tested in this study, R_0 and R_1 were chosen as 150 mm, and R_2 was chosen as 75 mm (i.e., $R_0 = R_1 = 2R_2 = 150$ mm). The thicknesses of concrete and steel rings were set as 75 mm and 12.5 mm, respectively, as recommended by AASHTO T334-08.

After demolding, the circular and elliptical ring specimens were sealed with double-layer aluminum tape on their outer circumferential surfaces immediately to allow drying from their top and bottom surfaces only. Then four strain gauges were attached to the inner surface of the steel ring. The ring specimens were moved into a standard curing chamber with 23℃ and 50% RH (see Fig. 2). Finally, a data acquisition system was connected to record the strain of the central steel ring. The age corresponding to the first crack formation in concrete can be determined by the sudden drop of the recorded strain of the steel ring. Four specimens were prepared for each condition, and the average cracking ages are listed in Table 1.

(a) Standard curing chamber (b) Circular and elliptical ring specimens

Fig. 2. Instrumented ring test set-up.

Table 1. Average cracking ages in days obtained from experiment.

Ring geometric profile	Concrete ring height		
	30 mm	50 mm	75 mm
Circular	19	24	--
Elliptical	14	21	--

It can be seen from the experimental results in Table 1, under drying from top and bottom surfaces, the ring specimen height has significant effects on its cracking age. For circular and elliptical rings, the cracking ages were delayed by 5 days and 7 days, respectively, when the height of the ring specimens increased from 30mm to 50 mm. However, in the case of 75 mm height, no cracks were observed in both circular and elliptical rings during the monitoring period of 28 days. In addition, elliptical ring specimens cracked much earlier than circular ring specimens with the height of 30 mm or 50 mm. It indicates that, compared with the circular ring, the elliptical profile can provide higher degree of restraint under drying from top and bottom surfaces.

2.3 Free shrinkage concrete prism tests

To reflect the free shrinkage characteristics of concrete ring specimens described in section 2.2, three series of free shrinkage prism tests with specimen sizes of 300 mm × 75 mm × 30 mm, 300 mm × 75 mm × 50 mm and 300 mm × 75 mm × 75 mm were conducted to measure free shrinkage strain of concrete. In all the three series of prismatic specimens, 300 mm is the length of the specimens. Two kinds of drying conditions were adopted in the free shrinkage prism tests (see Fig. 3(a)). In the case of the first drying condition, the prismatic specimens were dried from the two exposed 300 mm × 75 mm surfaces symmetrically, while the other surfaces were sealed by double-layer aluminum tapes. In the case of the second drying condition, the prismatic specimens with all surfaces sealed were tested to measure shrinkage strain caused by autogenous shrinkage. The magnitudes of free shrinkage were measured by using mechanical dial gauges (see Fig. 3(b)) and the deformation was recorded twice a day at regular base. By fitting the measured data, free shrinkage strains at different ages can be derived, which are graphically presented in Fig. 4.

(a) Three series of prism specimens with two drying conditions (b) Test setup

Fig. 3. Free shrinkage tests.

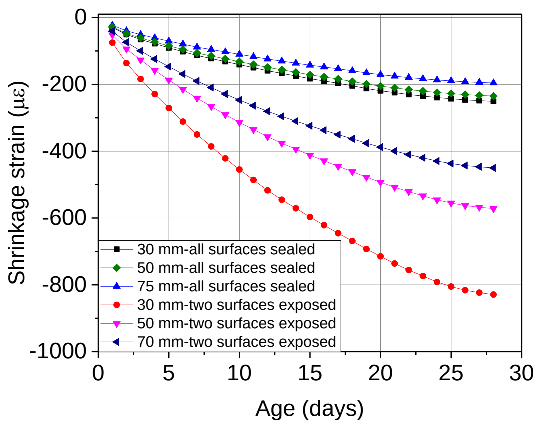

Fig. 4. Shrinkage strains of prism specimens in free shrinkage tests.

3 Numerical Simulations

Based on the experimental results, under drying from top and bottom surfaces, the specimen height has significant influence on the cracking age for both circular and elliptical ring profiles. This phenomenon happened for two reasons: (1) different ratios of the exposed area to volume (A/V) for different specimen heights affect the magnitude of shrinkage of concrete; and (2) the non-uniform shrinkage along the specimen height direction results in the bending effect in concrete. Particularly, the non-uniform shrinkage affects the crack initiation and propagation in concrete and makes the fracture mechanism in the ring test more complex. As a result, it is difficult to define the cracking state of concrete corresponding to the observed strain drop in the steel ring from the experiment. Therefore, it is necessary to investigate the influence of non-uniform shrinkage of concrete along the height direction on crack initiation and propagation, and clearly elucidate the fracture mechanism in the ring test under drying from top and bottom surfaces.

In this study, numerical analyses were carried out using ANSYS finite element software to investigate the fracture process for circular and elliptical rings with various heights under drying from top and bottom surfaces. In the numerical simulations, the fictitious temperature field, derived from free shrinkage tests, was applied in the numerical model to simulate the shrinkage effect of concrete. The fracture mechanics method based on the fictitious crack model [27] was introduced to study the fracture process of the concrete ring. To simulate the non-uniform shrinkage along the specimen height direction, three-dimensional finite element modeling was established. Considering the symmetry of specimen geometry and drying condition, a specimen model was established for only a quarter of the ring to reduce calculation time consumption by imposing restrictions on the symmetry planes.

3.1 Fracture model

A fictitious crack model [27] was introduced in the fracture analysis to characterize the nonlinear property of concrete by applying a cohesive force on the fracture process zone (FPZ). The bilinear expression [31] for the softening stress (σ) and crack opening displacement (w) relationship for concrete was used in the numerical simulation, which is illustrated in Fig. 5.

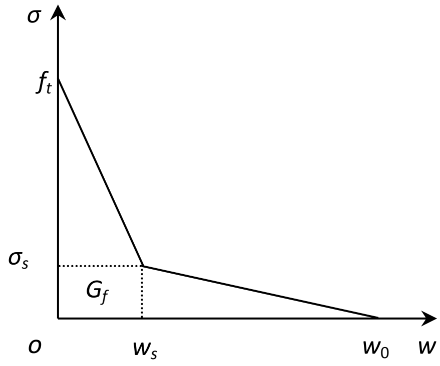

Fig. 5. Bilinear *σ*-*w* softening curve for concrete.

According to the research of Peterson [31], σ_s, w_s and w_0 can be determined as follows:

$$\sigma_s = f_t/3 \tag{5}$$

$$w_s = 0.8G_f/f_t \tag{6}$$

$$w_0 = 3.6G_f/f_t \tag{7}$$

where, w_0 is the stress-free crack opening displacement and w_s and σ_s are the displacement and stress corresponding to the break point in the bilinear *σ*-*w* relationship, respectively. The *σ*-*w* relationship can be determined once fracture energy G_f and tensile strength f_t of concrete are given.

A concrete crack propagation criterion based on the initial fracture toughness has been proposed and validated [32], which can determine the crack propagation during the whole fracture process of concrete [33]. In this study, this criterion was introduced to analyze crack initiation and propagation in the concrete rings subject to restrained shrinkage. This criterion can be described as following: a crack begins to propagate when the difference between the stress intensity factors (SIFs) caused by the shrinkage effect, K_I^S, and by the cohesive stress, K_I^σ, exceeds the initial fracture toughness of concrete, K_{IC}^{ini}. The criterion can be described as follows:

$$K_I^S - K_I^\sigma < K_{IC}^{ini}, \text{ crack does not propagate} \tag{8}$$

$$K_I^S - K_I^\sigma = K_{IC}^{ini}, \text{ crack is in the critical state} \tag{9}$$

$$K_I^S - K_I^\sigma > K_{IC}^{ini}\text{, crack propagates} \tag{10}$$

For any specific age, by applying the fictitious temperature field on concrete, the SIF K_I^S at the tip of the pre-crack can be calculated using the displacement extrapolation method. Further, the cohesive force can be derived from the bilinear *σ*-*w* relationship based on the crack opening displacement, and K_I^σ can be calculated accordingly. Thus, crack propagation status can be determined by comparing $K_I^S - K_I^\sigma$ with K_{IC}^{ini}. If Equation (10) is satisfied, cracks will propagate and a new numerical mode is established with a crack length increment of 2 mm. If not, the fictitious temperature field corresponding to the following day will be applied until the crack propagation condition is satisfied. It should be noted that all concrete material properties adopted in the numerical analyses are updated once a day.

3.2 Fictitious temperature field

In the restrained shrinkage ring test, concrete shrinkage is mainly caused by cement hydration (autogenous shrinkage) and moisture movement (drying shrinkage). Accordingly, for the ring specimen under drying from top and bottom surfaces, two fictitious temperature fields should be derived from the results of the free shrinkage tests to characterize shrinkage conditions: (1) uniform fictitious temperature field to characterize the autogenous shrinkage and (2) non-uniform fictitious temperature field to characterize the non-uniform drying shrinkage along the height direction.

The uniform temperature field can be derived from the shrinkage strain of a prismatic specimen with all surfaces sealed by dividing it by the coefficient of thermal expansion, 10×10^{-6}/℃. In this case, there is no moisture loss from the concrete specimen and the shrinkage strain is completely caused by cement hydration, i.e. autogenous shrinkage. For the non-uniform fictitious temperature field, it was assumed that it corresponds to the moisture distribution along the height direction of a ring specimen under drying from top and bottom surfaces. Based on the experimental investigations conducted by Weiss [34], the moisture distribution in a concrete specimen drying from a single surface at any position and at any age can be calculated by the following equation:

$$H(x,t) = H_{INTERNAL} - (H_{INTERNAL} - H_{EXPOSED})\left(10^{-(A_1 D + A_2) t^{(B_2 + B_1 \ln(D))} \frac{x}{D}}\right) \qquad (11)$$

where $H(x,t)$ is the relative humidity at the depth x from the drying surface, $H_{INTERNAL}$ is the internal relative humidity of the concrete specimen if it is completely sealed (in this paper, $H_{INTERNAL}$ was assumed to be 100%), $H_{EXPOSED}$ is the relative humidity at the exposed surface of the specimen. The coefficients A_1, A_2, B_1 and B_2 in Eq. (11) were determined as 0.2007, -1.0455, 0.0865 and -0.9115, respectively. D is the distance from drying surface. According to Moon et al. [14], the relationship between the drying shrinkage and moisture distribution within a concrete element can be assumed as linear. Therefore, the moisture distribution along the height direction in three series of ring specimens with the heights of 30 mm, 50 mm and 75 mm can be determined based on Eq. (11). Accordingly, the non-uniform fictitious temperature field can be derived by introducing the coefficient of thermal expansion for concrete to calculate the drying shrinkage strain. The derived fictitious temperature fields applied in the numerical model at 1, 3, 7, 14, 21, 28 days for three specimen heights are illustrated in Fig. 6.

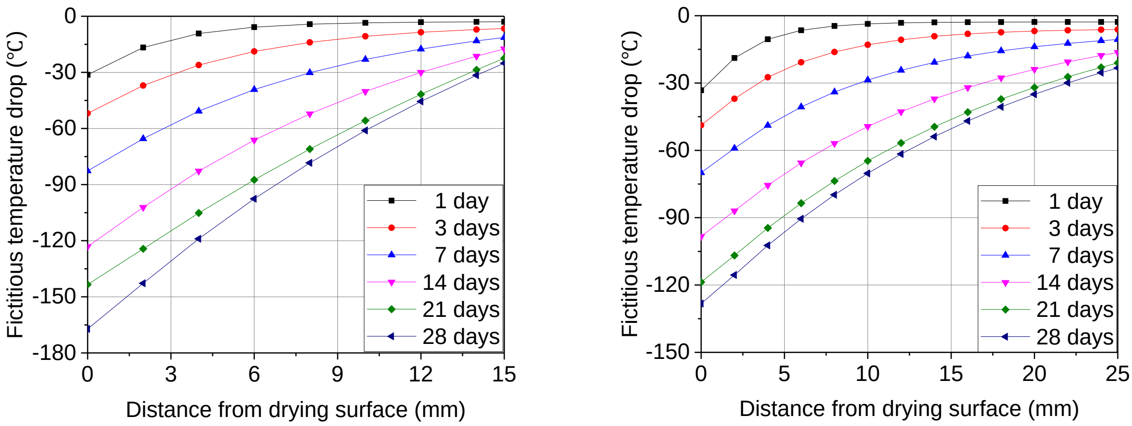

(a) 30 mm tall ring specimen (b) 50 mm tall ring specimen

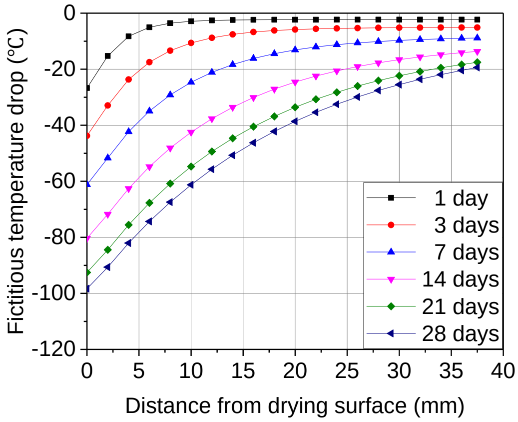

(c) 75 mm tall ring specimen

Fig. 6. Fictitious temperature fields applied on numerical models.

Taking the 50 mm height circular and elliptical ring specimens as examples, Fig. 7 shows the temperature field distributions along the height direction in the concrete ring on the 14th day. It can be seen that the largest fictitious temperature drop occurs at the exposed top surface and the fictitious temperature drop decreased gradually along the height direction in the concrete rings.

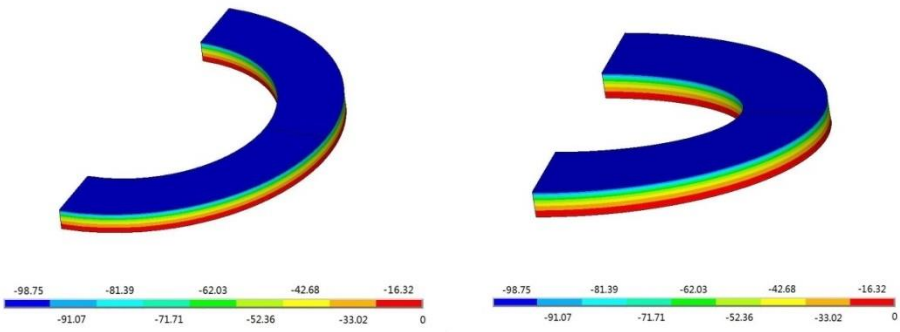

(a) Circular ring (b) Elliptical ring

Fig. 7. Fictitious temperature fields on the 14th day for ring specimens with 50 mm tall (Unit: ℃).

3.3 Determination of the position of the **initial crack**

When the tensile stress in concrete is greater than the tensile strength, cracking will initiate. Thus, the initial crack position can be determined through the distribution of the tensile stress in concrete. In the case of drying from top and bottom surfaces, tensile stress is caused by both the non-uniform shrinkage along the height direction and the restraint from the inner steel ring. A structural analysis was carried out to calculate the distribution of tensile stress in concrete after applying the non-uniform temperature field to simulate the effect of the moisture gradient in the thermal analysis. The elastic module of concrete was reduced by 40% to characterize the creep effect of concrete [17, 35]. In addition, the section of the first crack usually locates randomly along the circumference in a circular ring specimen and near major axis in an elliptical ring specimen due to geometrical effect. Figs. 8(a) and (b) illustrate the cracks in the circular and elliptical ring specimens, respectively. The tensile stress distributions in cross-sections of circular and elliptical rings (randomly along the radial direction for the circular ring and along the major axis for the elliptical ring) were calculated and derived, as shown in Figs. 9(a) and (b), respectively.

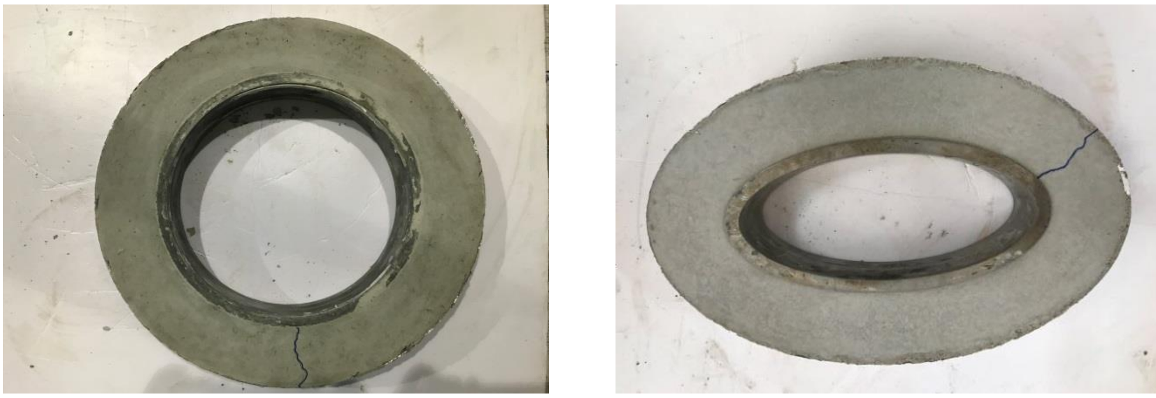

(a) Circular ring (b) Elliptical ring

Fig. 8. Cracks in circular and elliptical ring specimens with height of 50 mm.

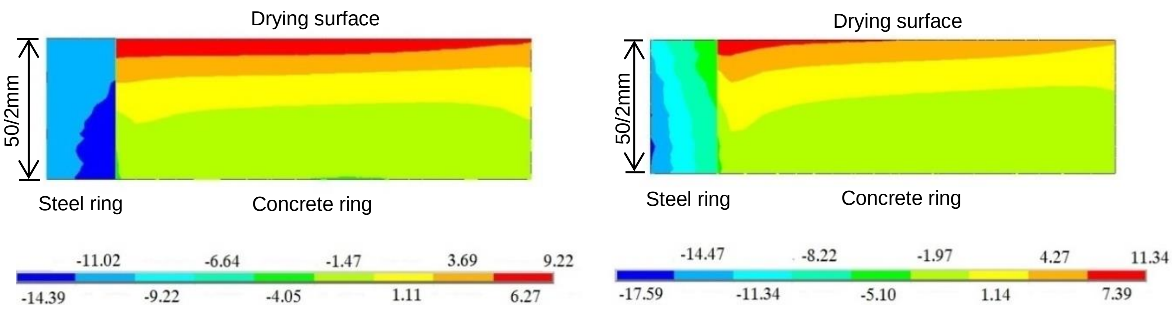

(a) Circular ring (b) Elliptical ring

Fig. 9. Stress contour along the cross-section of a 50 mm tall ring specimen on the 10th day (Unit: MPa).

It can be seen, for both circular and elliptical rings, tensile stress distributions are hierarchical in intensity along the height directions. The tensile stress reaches the highest at the top surface and decreases along the height direction down to median surface of the ring specimen. At the bottom of a cross-section, i.e. at half the height of a concrete ring, tensile stress turns into compressive stress. In addition, in the case of the same height, tensile stress near the inner steel ring surface is the highest and the maximum tensile stress occurs at the top left corner of the cross-sections (red zone in Figs. 9(a) and (b)). Therefore, it can be predicted that the first crack occurs at the top left corner of cross-section for the circular and elliptical specimens. According to previous research [30], the crack will propagate throughout the whole radial section immediately after being subject to uniform shrinkage along the radial direction. Therefore, the conclusion can be drawn that the first crack will occur at the exposed surface for the circular and elliptical concrete ring specimens under drying from top and bottom surfaces.

3.4 Crack propagation process

After the initial crack position is determined, a pre-crack with 2 mm long was set on the exposed surface along the radial direction for a circular ring and along the major axis for an elliptical ring. At that moment, there are two potential crack propagation directions, i.e. the crack propagates from the exposed surface along the height direction or from the inner circumference along the radial direction or major axis direction. However, it should be noted that the fracture mechanisms for the two crack propagation directions are different. The crack propagation along the height direction is mainly caused by the non-uniform shrinkage from the moisture gradient in the concrete. In contrast, the crack propagation along the radial direction is mainly caused by the restraint shrinkage from the inner steel ring. In order to clarify the fracture mechanism in the circular/elliptical ring tests, it is significant to investigate the crack propagation process under drying from top and bottom surfaces of a restrained concrete ring.

Firstly, it is assumed that the crack will propagate along the height direction. The fictitious temperature field derived from section 3.2 was applied to concrete and the cohesive stress was imposed on the initial crack. Corresponding to various ages, the differences in the SIFs at the tip of the initial crack caused by fictitious temperature field and by cohesive force, $K_I^S - K_I^\sigma$, were calculated from the 1st to 28th day. As an example, the results for circular and elliptical ring specimens with 50 mm tall are shown in Figs. 10(a) and (b), respectively.

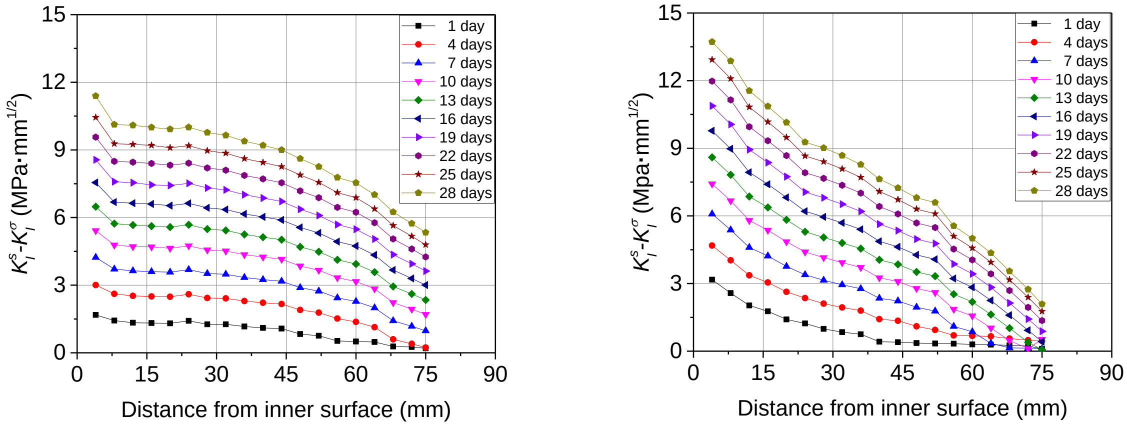

(a) Circular ring (b) Elliptical ring

Fig. 10. $K_I^S - K_I^\sigma$ at the tip of horizontal crack for the ring specimens with 50 mm tall.

It can be seen from this figure that the difference of SIFs, $K_I^S - K_I^\sigma$, increases with age. The maximum $K_I^S - K_I^\sigma$ occurs at the inner surface, and shows a slight descending trend along the radial direction. To determine the possibility of crack propagation along the height direction after crack initiation, the maximum values of $K_I^S - K_I^\sigma$ along the radial direction at different ages for elliptical ring specimens are shown in Fig. 11. It can be seen that, the maximum of $K_I^S - K_I^\sigma$ is less than the initial fracture toughness at each corresponding age (from 1 to 27 days), which indicates that the initial crack cannot propagate along the height direction under drying from top and bottom surfaces of a restrained concrete ring specimen.

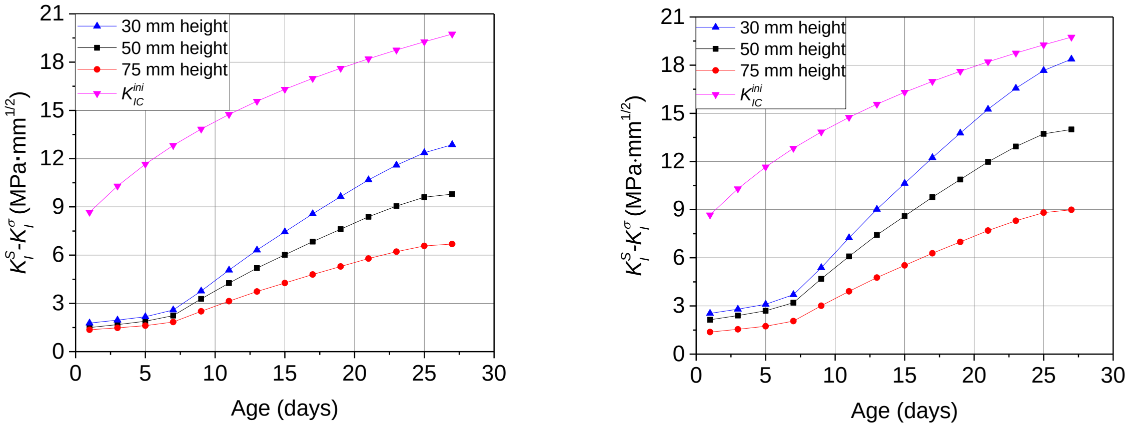

(a) Circular ring (b) Elliptical ring

Fig. 11 . Maximum $K_I^S - K_I^\sigma$ at the tip of horizontal crack for three series of ring specimens.

Following the latter result, the possibility of crack propagation from inner circumference along the radial direction will be investigated. In addition to the initial horizontal crack at the exposed surface along the radial direction, another vertical pre-crack was set at the inner circumference along the height direction. Figs. 12(a) and (b) show the values of $K_I^S - K_I^\sigma$ at the tip of the vertical cracks from 1 to 27 days for the circular and elliptical rings with 50 mm tall.

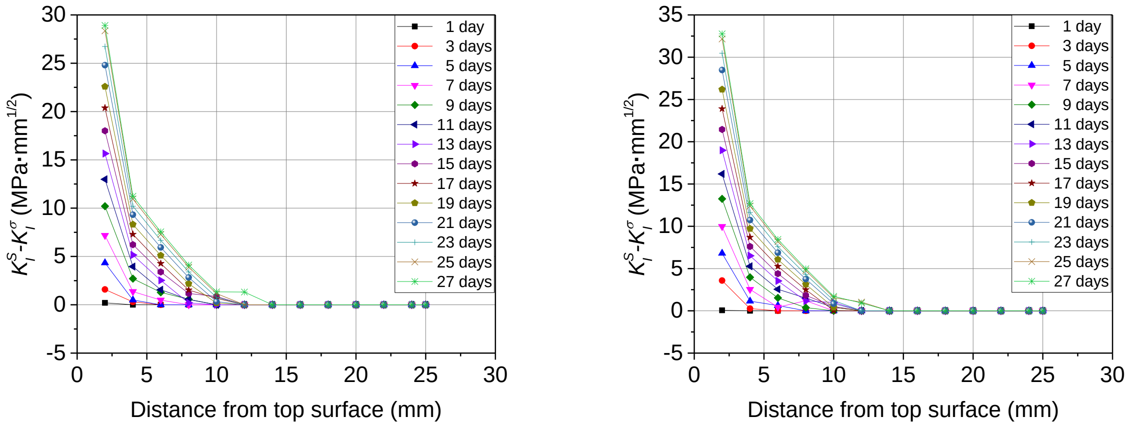

(a) Circular ring (b) Elliptical ring

Fig. 12. $K_I^S - K_I^\sigma$ at the tip of vertical crack for 50 mm tall ring specimens.

It can be seen from the figure that the maximum $K_I^S - K_I^\sigma$ at the tip of the vertical crack occurs at the top of the vertical crack (see Point A in Fig. 13(a)). However, the value of $K_I^S - K_I^\sigma$ corresponding to x = 10 mm in Fig. 12, i.e. near the inner circumference of concrete, significantly decreases along the height direction. It indicates that the crack cannot propagate completely along the cross-section from the inner to outer circumferences at the same age. Alternatively, it will propagate partly along the height direction and form a new horizontal penetrating crack until the vertical crack propagates throughout the whole cross-section. In order to investigate the whole crack propagation process, it was assumed that the Line AB (2 mm-long) of vertical crack (see Fig. 13(a)) will propagate to the outer surface (see Fig. 13(b)) when the average value of $K_I^S - K_I^\sigma$ at points A and B exceeds the initial fracture toughness at the corresponding age.

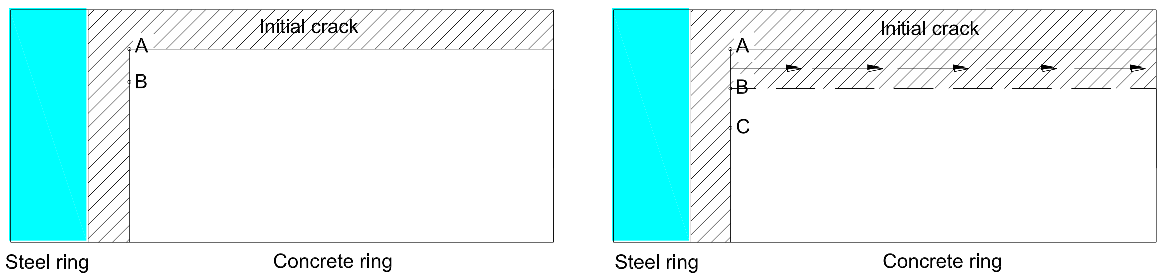

(a) Initial crack (b) Crack propagation path

Fig. 13. Cross-section of 50 mm tall ring specimens.

The average values of $K_I^S - K_I^\sigma$ at points A and B were calculated from 1 to 27 days for three series of ring specimens, which are illustrated in Fig. 14. It can be seen that the predicted ages corresponding to the AB part of the vertical crack started to propagate along the radial direction are 18 days and 24 days for circular rings with 30 mm and 50 mm tall, and 15 days and 19 days for elliptical rings with 30 mm and 50 mm tall, respectively. In addition, for circular and elliptical ring specimens with 75 mm tall, the Line AB of the vertical crack did not propagate at all during the 27-day monitoring period.

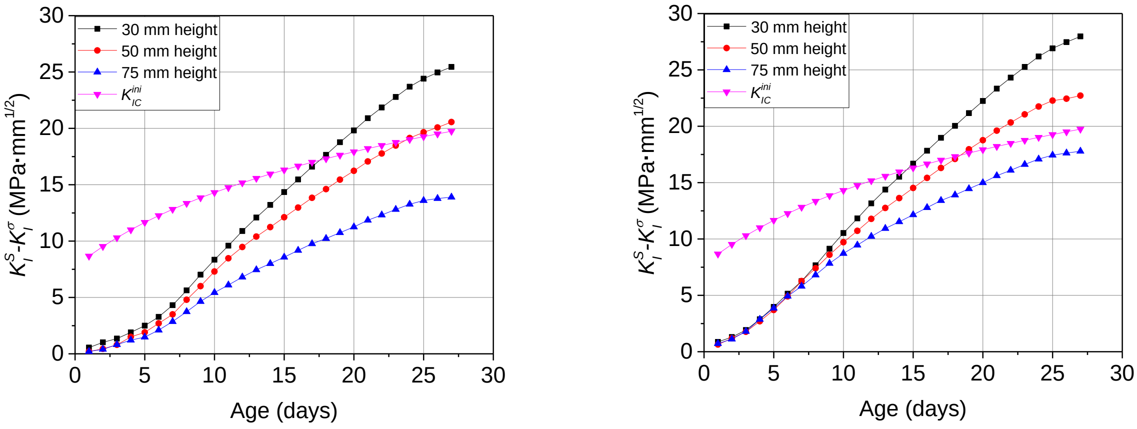

(a) Circular ring (b) Elliptical ring

Fig. 14. Average values of $K_I^S - K_I^\sigma$ at points A and B.

After the Line AB of the vertical crack propagates horizontally to the outer circumferential surface of concrete, a new model with a longer horizontal initial crack (i.e. Δ = 4 mm at that moment) was established (see Fig. 13(b)) to analyze whether the next 2 mm vertical crack, i.e. Line BC, can propagate continually. Accordingly, the variations of $K_I^S - K_I^\sigma$ at different heights for circular and elliptical rings with 30 mm and 50 mm tall are presented in Fig. 15.

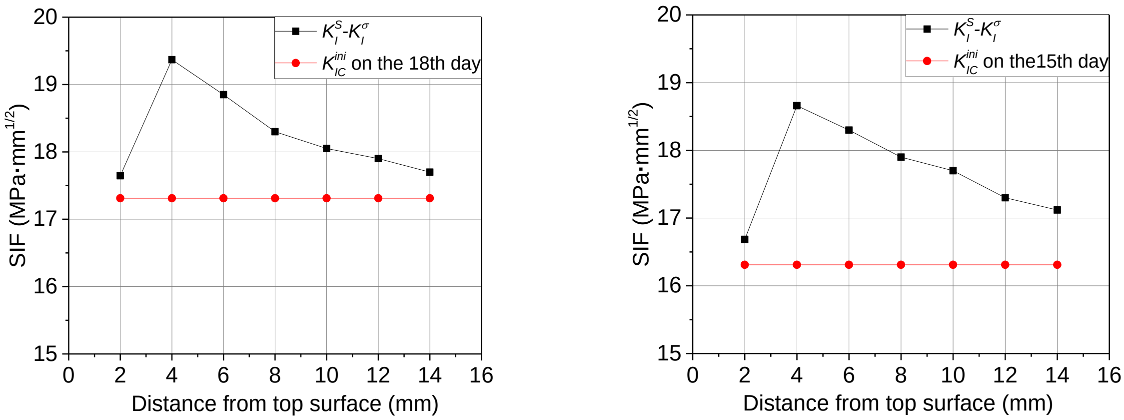

(a) 30 mm tall circular ring (b) 30 mm tall elliptical ring

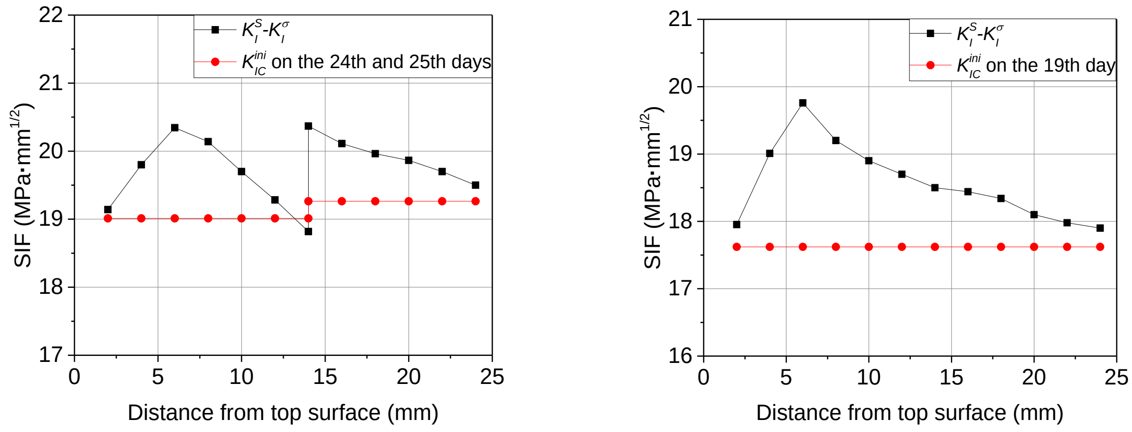

(c) 50 mm tall circular ring (d) 50 mm tall elliptical ring

Fig. 15. $K_I^S - K_I^\sigma$ during crack propagation process.

It should be noted that Figs. 15(a), (b) and (d) illustrate the relationship of $K_I^S - K_I^\sigma$ and K_{IC}^{ini} corresponding to the cracking age of Line AB. It can be seen that, after Line AB begins to propagate, the other vertical cracks with 2 mm length can propagate through their horizontal sections one by one until the whole crack section is formed. The scenario is slightly different in the case of a circular ring with 50 mm tall. The value of $K_I^S - K_I^\sigma$ is less than K_{IC}^{ini} when the crack length is 14 mm, which indicates that the crack cannot propagate throughout the section at the age when Line AB begins to propagate, i.e. at 24th day. However, the crack can form completely at the next age, i.e. at 25th day. The comparison of cracking ages obtained from numerical simulation and experiment shows a reasonable agreement (see Table 2), which verifies the established numerical analysis in this study.

Table 2. Cracking ages in days obtained from numerical simulation and experiment.

Ring geometric profile	Concrete ring height					
	30 mm		50 mm		75 mm	
	Exp.	Num.	Exp.	Num.	Exp.	Num.
Circular	19	18	24	25	--	--
Elliptical	14	15	21	19	--	--

4 Discussions

4.1 The influence of assumption on uniform shrinkage

It has been verified that the moisture gradient (consequently non-uniform shrinkage) along the height direction should be considered in analyzing the fracture process of ring specimens under drying from top and bottom surfaces. However, it should be noted that the moisture gradient is not significant as the specimen height decreases and the moisture can be regarded as uniformly distributed in the concrete ring. In this case, for the purpose of computational simplification, the uniform shrinkage assumption along the height direction is appropriate in the crack propagation analysis. It has been reported in previous research [21, 22] that the uniform shrinkage assumption along the height direction can be adopted approximately when the specimen height is 30 mm. However, it is not clear whether the assumption is still appropriate as the specimen height increases above 30 mm, e.g. 50 mm and 75 mm. In line with this, numerical analyses were conducted to investigate the fracture process of ring specimens with heights of 30 mm, 50 mm and 75 mm based on the assumption of uniform shrinkage. According to previous researches [15, 30], for a ring specimen subject to uniform shrinkage, the first cracking initiates at the inner circumference and propagates to the outer surface. Therefore, a 2mm long initial crack was set at the inner surface of the concrete ring, randomly along the radial direction for the circular ring specimen and along the major axis direction for the elliptical ring specimen. Meanwhile, following the uniform shrinkage assumption, specimen height only affects the ratio of the exposed area to volume (A/V), rather than the moisture gradient along the height direction. For ring specimens at each height, a prism with the same height was used to ensure the same A/V ratio. The uniform fictitious temperature field can be derived by dividing the free shrinkage strain of a two sides exposed prism specimen by the coefficient of thermal expansion of concrete (10×10^{-6}/℃). Fig. 16 illustrates the fictitious temperature drop for ring specimens with three different heights from 1 day to 28 days.

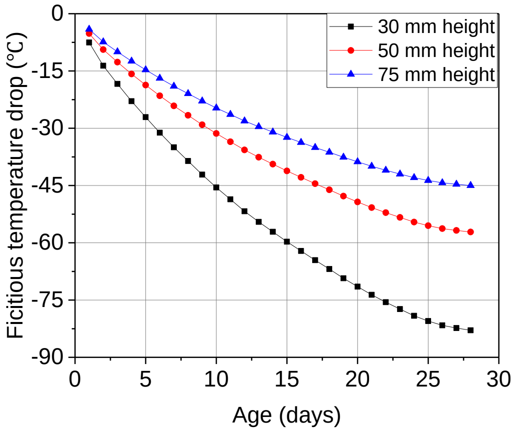

Fig. 16. Fictitious temperature drops based on uniform shrinkage assumption

Under a uniform temperature field condition, the relationship between $K_I^S - K_I^\sigma$ and K_{IC}^{ini} for circular and elliptical rings of three different heights are illustrated in Fig. 17(a) and (b), respectively.

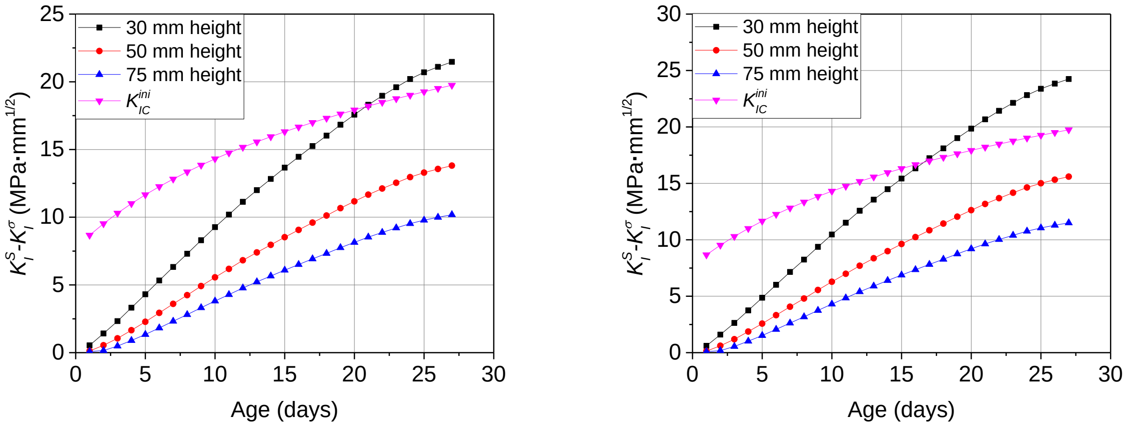

(a) Circular ring

(b) Elliptical ring

Fig. 17. $K_I^S - K_I^\sigma$ at the tip of the initial crack under uniform shrinkage

It can been seen that the elliptical and circular ring specimens with 30 mm tall cracked at ages of 17 and 21 days, respectively, which were appropriately the same as under the condition considering non-uniform shrinkage along the height direction (i.e. 15 and 18 days). However, both circular and elliptical rings with the height of 50 mm did not crack during the age of 28 days under the uniform shrinkage assumption, which is obviously different from the experimental results. Therefore, for the ring specimens with 30 mm tall, the cracking age can be approximately predicted by neglecting the moisture gradient along the height direction under drying from top and bottom surfaces. In the case of 50 mm and 75 mm heights, the effect of the moisture gradient is significant enough that cannot be neglected.

4.2 Quantitative analysis on the driving forces in crack propagation process: self-restraint vs. steel ring restraint

In the restrained shrinkage ring test, the shrinkage of concrete is restrained and tensile stress occurs in concrete, thus, driving the potential crack initiation and propagation. Generally, the restraint of the concrete ring consists of two parts, the self-restraint caused by non-uniform shrinkage and the external restraint from the steel ring. For a 75 mm thick ring specimen under outer circumference surface drying, it has been proved that crack propagation is mainly driven by the self-restraint rather than by the external restraint from steel ring due to significant non-uniform shrinkage along the radial direction [16]. In the case of drying from top and bottom surfaces, although the non-uniform shrinkage is partly reduced due to moisture diffusion from the two symmetrical surfaces, the effect of the moisture gradient is still significant for the ring specimens with 50 mm and 75 mm tall. In section 4.1, the uniform shrinkage assumption has been verified to be inappropriate for taller concrete ring specimens by comparing with the experimental results. Therefore, it was necessary to quantitatively analyze the effect of self-restraint and external restraint on crack propagation process in ring tests under drying from top and bottom surfaces of a restrained concrete ring.

It has been verified in this paper that the vertical cracks, e.g. Lines AB, BC… (see Fig. 13), will initiate and horizontally propagate to the outer circumference in turn until all vertical cracks propagate throughout the cross-section. Fig. 18 illustrates the SIFs of various vertical crack positions caused by self-restraint and steel restraint at the corresponding cracking age.

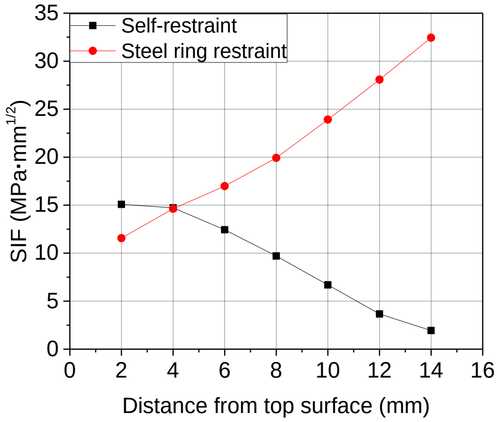

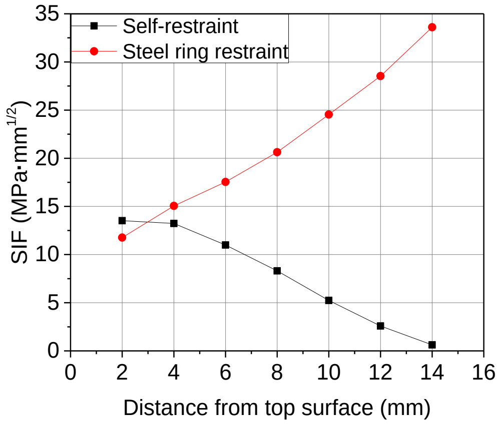

(a) Circular ring specimen with 30 mm tall (b) Elliptical ring specimen with 30 mm tall

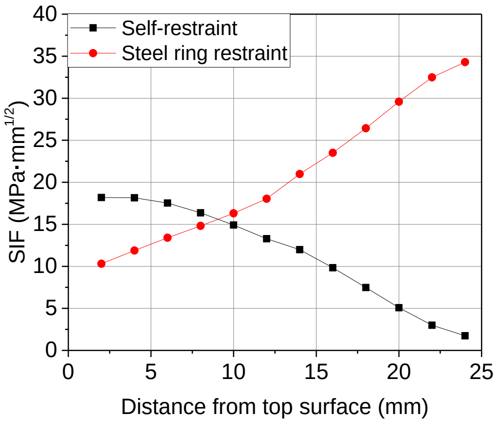

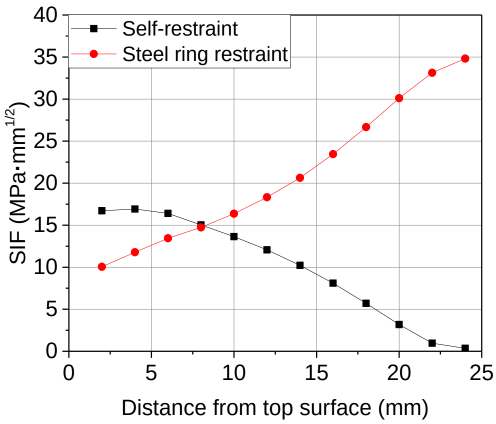

(c) Circular ring specimen with 50 mm tall (d) Elliptical ring specimen with 50 mm tall

Fig. 18. SIFs caused by self-restraint and steel ring restraint in crack propagation process corresponding to the cracking age.

It can be seen that, for each series of specimens, the first crack initiation, i.e. Line AB, is caused by both self-restraint and external steel ring restraint, and the proportion of self-restraint is greater than steel ring restraint. With the increase of distance from the top surface, the effect of self-restraint decreases while the effect of steel ring restraint increases. It indicates that the fracture mechanism is different for the crack initiation and propagation at various heights. The moisture gradient is significant near the top surface of a concrete ring, so, the bending effect caused by the non-uniform shrinkage is remarkable. In this case, the crack driving force is from both self-restraint and steel ring restraint. In contrast, the moisture gradient is not obvious as the crack propagates near the middle height between the top and bottom surfaces. In this case, the bending effect caused by the non-uniform shrinkage is very small and can be neglected, so the crack driving force is mainly provided by the steel ring restraint.

To study the component of the driving force at various heights, Fig. 19 illustrates the SIF ratio of $K_{I\ steel}^{S}$ to K_{I}^{S}. Here, $K_{I\ steel}^{S}$ is the SIF caused by steel ring restraint, and K_{I}^{S} is the SIF caused by the total restraint including self-restraint and steel ring restraint. It can be seen that, as the vertical crack initiates from top to bottom, the ratios of $K_{I\ steel}^{S}$ to K_{I}^{S} increase significantly. For circular and elliptical rings, the ratios do not present any obvious difference. However, compared with the concrete ring specimens of 30 mm tall, the proportion of self-restraint, i.e. the effect of the moisture gradient, becomes more significant for the specimen with 50 mm tall. This explains why uniform shrinkage assumption is inappropriate for a taller ring specimen under drying from its top and bottom surfaces.

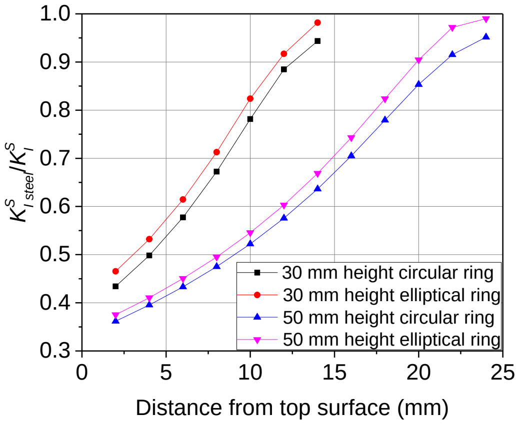

Fig. 19. Ratios of $K_{I\ steel}^{S}$ to K_{I}^{S} for concrete ring specimens with 30 mm and 50 mm tall.

5 Conclusions

The purpose of this paper is to investigate the influence of non-uniform shrinkage along the height direction on the fracture mechanism in restrained shrinkage circular/elliptical ring test under drying from top and bottom surfaces. Three series of ring specimens with heights of 30 mm, 50 mm and 75 mm were tested under restrained shrinkage conditions until cracking occurred or to the age of 28 days whichever is longer. By introducing the fictitious temperature field to simulate the shrinkage effect of concrete, a numerical approach based on fracture mechanics was developed to analyze the crack initiation and propagation process. Based on the experimental and numerical investigations, the following conclusions can be drawn:

(a) Under drying from top and bottom surfaces, cracking ages of elliptical ring specimens with 30 mm and 50 mm tall were 5 days and 3 days shorter than their counterpart circular ones, respectively. Although circular and elliptical ring specimens with 75 mm tall did not crack during the 28-day testing period, numerical results indicate that the elliptical ring geometric profile can provide greater values of $K_I^S - K_I^\sigma$ than the circular ring geometry profile. Therefore, the elliptical geometric profile can effective increase the restraining effect to shorten the cracking age of concrete and accelerate the process of restrained shrinkage test.

(b) The numerical method was verified by comparing the predicted cracking ages with those measured in experiment, showing a reasonable agreement. Based on the numerical analysis, under drying from top and bottom surfaces, the crack initiates partly at the inner circumference of the concrete ring and propagates along the radial direction. The fracture process is repeated until the crack propagates throughout the cross-section. For the circular and elliptical ring specimens with 30 mm and 50 mm heights, the cracks could form completely once the first crack initiated or in a very short period (about 1 day) after the first crack initiated.

(c) Under drying from top and bottom surfaces, the moisture gradient along the height direction had a significant effect on the fracture process of the concrete ring. The driving force of crack propagation was dominated by both moisture gradient and steel restraint when the crack initiates near the exposed surface of the ring specimen. With the increase of distance from the exposed surface, the effect of the steel ring restraint increased and the moisture gradient decreased. When the crack initiated near the middle height of top and bottom surfaces, the fracture process was mainly dominated by the steel ring restraint.

(d) For the ring specimens with 30 mm tall, the assumption of uniform shrinkage along the height direction can be approximately used to predict the cracking age, which is in a reasonable agreement with the results considering the non-uniform shrinkage. In the case of 50 mm height, the predicted cracking age based on the uniform shrinkage assumption is obviously different from the results based on the non-uniform shrinkage and the results from the experiment as well. However, it should be noted that, although the predicted cracking ages are similar based on the two assumptions, the fracture mechanisms are invariably different. In the assumption of uniform shrinkage, the contribution of non-uniform shrinkage on the driving force of crack propagation is not considered in the fracture analysis.

Acknowledgement

The financial support of the National Natural Science Foundation of China under the grants of NSFC 51478083, NSFC 51421064 and NSFC 51109026, UK Engineering and Physical Sciences Research Council under the grant of EP/I031952/1, and the Natural Science Foundation of Liaoning Province of China under the grant of 20170540183 is gratefully acknowledged.

References

[1] Wang K, Jansen DC, Shah SP, Karr AF. Permeability study of cracked concrete. Cem Concr Res 1997;27:381-93.

[2] Kovler K. Testing system for determining the mechanical behaviour of early age concrete under restrained and free uniaxial shrinkage. Mater Struct 1994;27:324-30.

[3] Altoubat SA, Lange DA. Creep, shrinkage, and cracking of restrained concrete at early age. ACI Mater J 2001;98:323-31.

[4] Weiss WJ, Yang W, Shah SP. Shrinkage cracking of restrained concrete slabs. J Eng Mech, ASCE 1998;124:765-74.

[5] Yang W, Weiss WJ, Shah SP. Predicting shrinkage stress field in concrete slab on elastic subgrade. J Eng

Mech, ASCE 2000;126:35-42.
[6] Collins F, Sanjayan JG. Numerical modeling of alkali-activated slag concrete beams subjected to restrained shrinkage. ACI Mater J 2000;97:594-602.
[7] Collins F, Sanjayan JG. Cracking tendency of alkali-activated slag concrete subjected to restrained shrinkage. Cem Concr Res 2000;30:791-8.
[8] Kawashima S, Shah SP. Early-age autogenous and drying shrinkage behavior of cellulose fiber-reinforced cementitious materials. Cem Concr Comp 2011;33:201-8.
[9] Emmanuel KA, Heather TS, Matthew AM. Potential for restrained shrinkage cracking of concrete and mortar. Cem Concr Aggr 2004;26:1-8.
[10] Kim B, Weiss WJ. Using acoustic emission to quantify damage in restrained fiber-reinforced cement mortars. Cem Concr Res 2003;33:207-14.
[11] Bentur A, Kovler K. Evaluation of early age cracking characteristics in cementitious systems. Mater Struct 2003;36:183-90.
[12] Wiegrink K, Marikunte S, Shah SP. Shrinkage cracking of high-strength concrete. ACI Mater J 1996;93:409-15.
[13] See HT, Attiogbe EK, Miltenberger MA. Shrinkage cracking characteristics of concrete using ring specimens. ACI Mater J 2003;100:239-45.
[14] Moon JH, Weiss J. Estimating residual stress in the restrained ring test under circumferential drying. Cem Concr Comp 2006;28:486-96.
[15] Hossain AB, Weiss J. The role of specimen geometry and boundary conditions on stress development and cracking in the restrained ring test. Cem Concr Res 2006;36:189-99.
[16] Dong W, Zhou X, Wu Z, Kastiukas G. Effects of specimen size on assessment of shrinkage cracking of concrete via elliptical rings: Thin vs. thick. Comput Struct 2016;174:66-78.
[17] Moon J-H, Rajabipour F, Pease BJ, Weiss J. Quantifying the influence of specimen geometry on the results of the restrained ring test. J ASTM Int 2006;3:1-14.
[18] Radlinska A, Pease B, Weiss J. A preliminary numerical investigation on the influence of material variability in the early-age cracking behavior of restrained concrete. Mater Struct 2007;40:375-86.
[19] Dean SW, Radlinska A, Bucher BE, Weiss J. Comments on the Interpretation of Results from the Restrained Ring Test. J ASTM Int 2008;5:1-12.
[20] Hossain AB, Weiss J. Assessing residual stress development and stress relaxation in restrained concrete ring specimens. Cem Concr Comp 2004;26:531-40.
[21] Weiss W, Shah S. Restrained shrinkage cracking: the role of shrinkage reducing admixtures and specimen geometry. Mater Struct 2002;35:85-91.
[22] Weiss WJ, Yang W, Shah SP. Influence of specimen size/geometry on shrinkage cracking of rings. J Eng Mech, ASCE 2000;126:93-101.
[23] Passuello A, Moriconi G, Shah SP. Cracking behavior of concrete with shrinkage reducing admixtures and PVA fibers. Cem Concr Comp 2009;31:699-704.
[24] Shah SP, Ouyang C, Marikunte S, Yang W, Becq-Giraudon E. A method to predict shrinkage cracking of concrete. ACI Mater J 1998;95:339-46.
[25] Dong W, Zhou X, Wu Z. A fracture mechanics-based method for prediction of cracking of circular and elliptical concrete rings under restrained shrinkage. Eng Fract Mech 2014;131:687-701.
[26] Xu S, Reinhardt HW. Determination of double-K criterion for crack propagation in quasi-brittle fracture, part II : Analytical evaluating and practical measuring methods for three-point bending notched beams. Int J Fract 1999;98:151-77.

[27] Hillenborg A, Modeer M, Petersson P. Analysis of crack formation and crack growth in concrete by means of fracture mechanics and finite elements. Cem Concr Res 1976;6:773-82.
[28] He Z, Zhou X, Li Z. New experimental method for studying early-age cracking of cement-based materials. ACI Mater J 2004;101:50-6.
[29] Zhou X, Dong W, Oladiran O. Experimental and numerical assessment of restrained shrinkage cracking of concrete using elliptical ring specimens. J Mater Civ Engng, ASCE 2014;26:4014087.
[30] Dong W, Zhou X, Wu Z, Xu B. Investigating crack initiation and propagation of concrete in restrained shrinkage circular/elliptical ring test. Mater Struct 2017;50:1-13.
[31] Petersson PE. Crack growth and development of fracture zones in plain concrete and similar materials Report TVBM-1006. Sweden: Division of Building Materials, Lund Institute of Technology; 1981.
[32] Dong W, Wu Z, Zhou X. Calculating crack extension resistance of concrete based on a new crack propagation criterion. Constr Build Mater 2013;38:879-89.
[33] Dong W, Zhou X, Wu Z. On fracture process zone and crack extension resistance of concrete based on initial fracture toughness. Constr Build Mater 2013;49:352-63.
[34] Weiss WJ. Prediction of early-age shrinkage cracking in concrete elements: Northwestern University; 1999.
[35] Kovler K. Drying creep of concrete in terms of the age-adjusted effective modulus method. Mag Concr Res 1997;49:345-52.